A Novel Scaling Process for the Computation of Multiconductor Transmission-Line Modal Properties Using the Basis Invariance of Total Current and Power

STUART BARTH, (Member, IEEE), AND ASHWIN K. IYER, (Senior Member, IEEE)
Department of Electrical and Computer Engineering, University of Alberta, Edmonton, AB T6G 1H9, Canada

Corresponding author: Stuart Barth (sbarth@ualberta.ca)

ABSTRACT It is generally regarded that some properties of the characteristic modes of multiconductor transmission lines, such as per-unit-length impedance, admittance, or characteristic impedance, cannot be meaningfully computed analytically. This inability arises from the nature of the definition of the modes – sets of relative voltages and/or currents – which in the prevailing understanding may be arbitrarily scaled. Several methods with which to compute scaling factors have been proposed, but often – and as demonstrated in this work – the results of these processes do not agree with values determined directly from field quantities or experiments. This work begins by examining several facets of multiconductor-transmission-line modes under the approximation of ideal TEM propagation: firstly, that transmission-line modes are normal, and secondly, that as a result of possessing this property, it is postulated that total currents in the terminal domain may be directly equated to those in the modal domain. It is then shown that these relations allow the scaling factors to be determined to within a sign, and as a result, modal properties may be directly computed. This technique allows for the extraction of the modal transmission-line properties for any arbitrary system of conductors. Multiple examples are studied numerically, in which it is shown that the proposed process results in much stronger agreement with field solution than other proposed processes, and further validation of the proposed process is provided though experimentally obtained data.

INDEX TERMS Characteristic impedance, characteristic modes, decoupling, diagonalization, modal analysis, multiconductor transmission-line.

I. INTRODUCTION

Transmission-line (TL) theory is a powerful concept that allows the fields of transverse electromagnetic (TEM) modes to be expressed as unique voltages and currents, making it a critical tool for high-accuracy circuit design. Basic TL systems contain only two conductors, whereas *multiconductor* TL (MTL) systems generally contain three or more conductors. The two common representations (strictly, bases, or ''domains'', in which the quantities are expressed) of MTLs are as follows:

1) The *terminal* domain (also referred to as the *natural* domain), in which the various TL parameters are

The associate editor coordinating the review of this manuscript and approving it for publication was Giorgio Montisci.

defined between each conductor and a pre-selected, common reference conductor. These parameters are expressed as dense matrices that are generally fully populated, implying that the various quantities evaluated on each conductor are in general coupled with each other.

2) The *modal* domain (also referred to as the *diagonalized* or *decoupled* domain), in which a TL's properties are given in terms of the TL's characteristic modes (also referred to as *propagation* modes) and expressed as diagonal matrices. The diagonality of the matrices implies that the solutions are isolated from one another and, due to this fact, each mode may be considered akin to a that of a simple two-conductor TL.

Terminal-domain parameters may be transformed into the modal domain via diagonalization, and vice-versa [1]–[3]. This change of basis requires the use of *transformation* matrices, which relate the propagating currents or voltages between the two domains. These matrices are sets of eigenvectors, implying that their exact values are known only to within a scale factor. This fact has historically resulted in the conclusion that some modal properties such as characteristic impedance, for which the scale factors do not cancel, cannot be determined when transformed from the terminal domain (although other methods may of course be used to obtain these values, such as derivation from known modal field quantities [1], [2], [4]–[6]).

Over roughly the last two decades, solutions have been proposed in attempts to overcome this ambiguity [7]–[10], and present similar processes to what will be introduced in this work, but generally either use ambiguous normalizations that lack physical bases, or produce sets of possible results.

The main contribution of this work is to demonstrate that any such ambiguities can be resolved by noting that physical quantities – specifically, total current – must be respectively equal in both domains, since the transformation between them is simply a change of basis. These physical constraints are used together to eliminate the unknown eigenvector scaling factors to within a sign and produce modal properties. The novelty of the work is validated through comparison with existing scaling methods, where it is found that the proposed method both produces characteristic impedance results that are in much closer agreement with numerical full-wave simulator HFSS, and also produces modal impedance values which are confirmed through experiment.

More recently, it was claimed that modal values could not be determined from terminal-domain equivalents, fundamentally due to the complex nature of the transformation matrices [11]. While this claim is surely valid if the transformation matrices are assumed generally complex, it is further demonstrated in this work that TL modes – under the assumption of transverse electromagnetic (TEM) propagation (referred to hereon as the *TEM approximation*) – are strictly *normal*, which allows these matrices to always be expressed as entirely real [3], [12].

The layout of this document is as follows: Sec. II begins with a brief discussion on the validity of the TEM approximation under quasi-TEM conditions, followed by the analytical process of the terminal-to-modal transformation. Section II concludes with the derivation of the source of the ambiguous scale factors and a brief overview of previously proposed solutions. Background on the requirement that TL modes are normal, and the application of the postulate of equality of total charges to solving modal properties are presented in Sec. III. Section IV presents full-wave simulation data for two different MTLs (one canonical, and the other designed as a lossy, asymmetric case meant to demonstrate the versatility of the proposed method), and demonstrates how modal per-unit-length properties may be directly computed using only the terminal-domain per-unit-length values. The predicted

modal characteristic impedances of one of these MTLs are experimentally validated in Sec. V. Lastly, the key findings and proposed applications are summarized in Sec. VI.

As demonstrated in this work, the determination of modal properties allows for, among a variety of other applications, the matching of MTLs of differing geometries, even those possessing different numbers of conductors and constructed around different dielectrics, which is currently only possible via parametric optimization or the use of a limited set of closed-form expressions. Additionally, modern applications of MTL theory, such as the analysis and design of periodic MTL metamaterials [13]–[17] would benefit greatly from the process proposed in this work, since it would allow for the direct determination of *Bloch* modal properties, such as Bloch impedance and effective constitutive medium parameters, for periodic structures in which lumped reactive elements can be incorporated into a host MTL. The properties at present may only be determined through laborious analytical solutions or extraction from the scattering of a finite array of structures [18], [19], where it may be excessively difficult to properly excite each mode and a small error will always be present due to the finite extent of the array.

II. BACKGROUND
A. THE TEM APPROXIMATION
TL theory is able to express the electric and magnetic field vectors of a given TL mode as scalar voltages and currents through the application of various properties of TEM modes [1], [2]. The TEM condition requires that a TL's conductors have identically zero resistivity, and that the TL is embedded in a homogenous medium. The former condition requires superconductivity, which is rather uncommonly encountered in practical systems, while the latter can only be realized in a completely enclosed system. These conditions – if met – ensure that TL modes do not possess longitudinal field components; however, it is commonly taken that in many practical cases the longitudinal field components may be ignored since they are much smaller than their tangential counterparts. This assumption gives rise to the TEM approximation, in which results derived for strictly ideal TEM cases may be applied to realistic, quasi-TEM TL modes.

The TEM approximation will be used in exactly the same spirit in this work: that is, the derivations made assuming TEM conditions are presumed to hold in the cases of mild conductor losses and/or inhomogeneous media – with some small, but tolerable error being incurred as a result (it is noted here that all of the practical examples given in Sec. IV reasonably satisfy the TEM approximation).

B. PROPAGATION IN THE TERMINAL DOMAIN
Currents and voltages propagating along a MTL in the z-direction may be expressed as [1]

$$\frac{\partial}{\partial z} \vec{V}_T = -[Z_T] \vec{I}_T \tag{1a}$$

$$\frac{\partial}{\partial z} \vec{I}_T = -[Y_T] \vec{V}_T \tag{1b}$$

where $[Z_T]$ and $[Y_T]$ are the per-unit-length impedances and admittances. Combining (1a) and (1b) yields the voltage and current Helmholtz equations,

$$\frac{\partial^2}{\partial z^2}\vec{V}_T = [Z_T][Y_T]\vec{V}_T \tag{2a}$$

$$\frac{\partial^2}{\partial z^2}\vec{I}_T = [Y_T][Z_T]\vec{I}_T \tag{2b}$$

where the products $[Z_T][Y_T]$ and $[Y_T][Z_T]$ may be expressed as the squares of the propagation constant matrices:

$$\left[\gamma_{VT}\right]^2 = [Z_T][Y_T] \tag{3a}$$

$$\left[\gamma_{IT}\right]^2 = [Y_T][Z_T] \tag{3b}$$

At a given plane (e.g., $z = 0$), the forward- and backward-travelling components of voltages and currents sum to the total:

$$\vec{V}_T = \vec{V}_T^+ + \vec{V}_T^- \tag{4a}$$

$$\vec{I}_T = \vec{I}_T^+ + \vec{I}_T^- \tag{4b}$$

and characteristic impedances $[Z_{cT}]$ are defined by the forward- or backward-travelling voltage and current waves

$$\vec{V}_T^+ = [Z_{cT}]\vec{I}_T^+ \tag{5a}$$

$$\vec{V}_T^- = -[Z_{cT}]\vec{I}_T^- \tag{5b}$$

Inserting (4) into (5) using (1) and (3), it may be shown that

$$[Z_{cT}] = \left[\gamma_{VT}\right]^{-1}[Z_T] \tag{6a}$$

$$[Z_{cT}] = [Z_T]\left[\gamma_{IT}\right]^{-1} \tag{6b}$$

C. MODAL-DOMAIN QUANTITIES

The characteristic modes of a MTL are defined as those for which all of the voltages and currents incur phase at the same rate – i.e., they are the voltages and currents that satisfy (2a) and (2b) [3], [20]. In these cases, the solutions to these equations are typically of the following form (although there exist some extremely uncommon pathological exceptions [21]):

$$\vec{V}_T(z) = \vec{V}_T^+ e^{-\gamma_M z} + \vec{V}_T^- e^{\gamma_M z} \tag{7a}$$

$$\vec{I}_T(z) = \vec{I}_T^+ e^{-\gamma_M z} + \vec{I}_T^- e^{\gamma_M z} \tag{7b}$$

where the propagation constants γ_M are those associated with each characteristic mode. Inserting these solutions back into (2a) and (2b) yields the characteristic equations:

$$\gamma_M^2 \vec{V}_T = [Z_T][Y_T]\vec{V}_T \tag{8a}$$

$$\gamma_M^2 \vec{I}_T = [Y_T][Z_T]\vec{I}_T \tag{8b}$$

Equations (8a) and (8b) may be recognized as eigenmode equations, and are typically solved via standard numerical processes. In these cases, the eigenvalues are the squares of the modal propagation constants, while the eigenvectors are the sets of relative currents and voltages associated with each of these eigenmodes.

Expanding on the notion of the eigenvectors, it is typical to relate the voltages and currents on each conductor

(i.e., the terminal-domain voltages and currents) to weighted sums of voltages and currents of the eigenvectors (i.e., the *modal* voltages and currents $\vec{V}_M$ and $\vec{I}_M$). That is, if the matrices $[T_V]$ and $[T_I]$ are the eigenvectors of (8a) and (8b), respectively:

$$\vec{V}_T = [T_V]\vec{V}_M \tag{9a}$$

$$\vec{I}_T = [T_I]\vec{I}_M \tag{9b}$$

These relations are the critical link in establishing the modal-domain properties, and their transformation from the terminal domain. For these reasons, $[T_V]$ and $[T_I]$ shall be referred to as the voltage and current "transformation matrices", respectively. Inserting these definitions into (1), (2), and (5), and comparing with their terminal-domain counterparts, yields the well-known relations:

$$[Z_M] = [T_V]^{-1}[Z_T][T_I] \tag{10a}$$

$$[Y_M] = [T_I]^{-1}[Y_T][T_V] \tag{10b}$$

$$[\gamma_M]^2 = [T_V]^{-1}[Z_T][Y_T][T_V] \tag{11a}$$

$$[\gamma_M]^2 = [T_I]^{-1}[Y_T][Z_T][T_I] \tag{11b}$$

$$[Z_{cM}] = [T_V]^{-1}[Z_{cT}][T_I] \tag{12}$$

which are necessarily diagonal matrices (when the characteristic modes exist [21]). Other modal properties of MTLs may be determined in a similar manner.

D. ORIGINS OF AMBIGUITY

Equations (10) through (12) specify that modal properties may be simply derived from a combination of terminal-domain data and transformation matrices. Since the terminal-domain data are unambiguously correct, any ambiguity in the modal-domain definitions must be inherited from transformation matrices themselves. Considering the matrices $[T_V]$ and $[T_I]$ in detail, it may be observed through (9) that each column of these matrices is a vector that relates currents and voltages on each conductor to the excitation of a single mode. Such a vector shall be referred to as a "mode definition", with the set of all mode definitions composing the transformation matrices. Equations (10) through (12) specify that each mode definition is associated with various properties, such as scalar impedance, admittance, propagation constant, and characteristic impedance.

Because each mode definition is an eigenvector derived from (8), the definitions may be arbitrarily scaled by any scalar value. Inserting these scale factors into either of (11) yields an intriguing conclusion: the modal propagation constants are not affected by any scaling applied to the mode definitions. Because of this fact, there is consensus that the propagation constants of a MTL's characteristic modes are well defined, and uniquely determinable. However, the same cannot be said of (10) and (12). In these equations, any scale factor applied to the mode definitions does not cancel out, and thus the modal per-unit-length impedance, admittance, and characteristic impedances are directly and significantly

affected by any arbitrarily chosen scale factor. As a consequence of this fact, it has been historically agreed upon that these modal quantities cannot be determined [1], [2], [7], [11]. Still, the following section details some scale factors that have previously been introduced in order to align the calculated values of these modal properties with those determined via other methods, such as analytical or numerical field integrations.

E. EXISTING SCALING PROCESSES
Presently, there exist some strategies for constraining the transformation matrices in attempt to determine the appropriate scale factors. Two of the most common are based on simple normalizations that are typically arbitrarily chosen and applied; both were detailed extensively in [7]. The first is the normalization of the product $[T_V]^T [T_I]$, for which it was shown that the symmetric nature of $[\gamma_M]^2$, $[Z_T]$, $[Y_T]$ leads to the conclusion that

$$[T_I]^T [T_V] = [T_V]^T [T_I] = [D], \qquad (13)$$

where $[D]$ is any diagonal matrix, typically (and arbitrarily) chosen to be identity for convenience. The second method involves a form of self-normalization of the matrix diagonals, such that

$$[T_I]^T [T_I] = [T_V]^T [T_V] = [I] \qquad (14)$$

Some work has also been done in attempting to normalize via physical quantities such as voltage, current, and power [10], [22]; however, the processes in [10] are not examined in the context of producing modal values, while those in [22] do not produce unique results for a given geometry.

F. SPECIAL CASES: REPEATED AND INDETERMINABLE EIGENVALUES
It must be noted that a suitable diagonalization to determine modal quantities may not always be possible [1], [2], [21], [23]. The cases of non-diagonalizable matrices (equivalently, the non-existence of characteristic modes), will not be investigated, nor will the cases of repeated eigenvalues in TEM systems be explicitly studied. It is important to clarify that this works seeks to demonstrate that modal properties may be accurately determined analytically, given specific mode definitions.[1]

G. COMPUTATION FROM NUMERICAL FULL-WAVE SOLVERS
The properties of MTL modes may be determined directly from numerical full-wave solvers. For example, in an eigenmode simulation of a TL's transverse cross-section, electric ($\vec{E}$) and magnetic ($\vec{H}$) fields are present, which not only allow for the computation of power, but also currents and

---

[1]As to how those modes are determined in difficult and uncommon scenarios is outside the scope of this work, but the interested reader is referred to [1], [2], [21], [23].

voltages, through integration of the fields along appropriate paths [4]–[6], [22], [24]–[26].

The modal properties may then be defined in terms of these quantities; e.g., characteristic impedance is famously computed from both voltage and current ("VI"), or power and current ("PI"), or power and voltage ("PV"). The reason these different definitions exists is that typically quasi-TEM modes are being solved for. For strictly TEM modes, all of these methods will return the same results; however, for quasi-TEM modes the $\vec{E}$ and $\vec{H}$ fields possess some non-negligible longitudinal components, and definitions of voltage and current are not unique. However, once again, the variation in results produced by the differing methods is seen to be satisfactorily small for most quasi-TEM modes [9]; in other words, the (tolerable) error in the large majority of quasi-TEM cases justifies the use of the TEM approximation.

III. SOLUTION PROCESS
A. INITIAL POSTULATES AND TERMINOLOGY
Modal-terminal domain transformations rely on the fact that both domains are equally valid representations of the same physical system. Therefore, various physical properties must be equivalent in both domains, foremostly, total energy and total current (charge); that is, these properties must be invariant to any change in basis such as $\vec{I}_T \rightarrow \vec{I}_M$. In the frequency domain, these are directly related to total power and current. It is well known and accepted that power is equal between terminal and modal domains; however, there exists some confusion in the literature as to whether this applies to *total* (i.e., complex) power [11] or instead the real, or time-averaged power [7], which affects the ability to determine mode definitions. Therefore, it will be demonstrated that complex power is equivalent in both domains, which is a direct consequence of one set of restrictions on the scaling factors of the transformation matrices. This will be elaborated on in Sec. III-C. The second restriction is established via postulate, where it is taken that

> The total currents of a given phase in the modal domain are equal to the total of those of the same phase in the terminal domain.

This will be investigated in Sec. III-D. The reader may note that the abovementioned postulate does not, in any way, restrict the phase relationship between currents in a given domain. In order to apply the equality of currents between domains, it is necessary to first demonstrate also that the currents of the characteristic modes may be separated into co- and contra-directed sets. Such a behavior is a characteristic of *normal* modes, in which all field points are simultaneously either in-phase or 180° out-of-phase. It is shown in the following section that TL modes (that is, those under the TEM approximation) must be normal.

While the total voltages and currents in the terminal domain ($\vec{V}_T$ and $\vec{I}_T$, respectively) generally represent a superposition of excited modes, it will be of interest to examine the effects of a single excited mode in the terminal domain. In this

case, these terminal voltages and currents will be expressed as

$$\vec{V}_T\Big|_n = [T_V]\,\vec{\delta}_n V_{Mn} \tag{15a}$$

$$\vec{I}_T\Big|_n = [T_I]\,\vec{\delta}_n I_{Mn} \tag{15b}$$

where V_{Mn} and I_{Mn} are the voltage and current of the excited mode n, respectively, and the delta vector $\vec{\delta}_n$ is defined as

$$\vec{\delta}_n = \begin{cases} 1, & \text{if } i = n \\ 0, & \text{otherwise} \end{cases} \quad \forall \text{ indices } i. \tag{16}$$

The inner product will be used to represent sums over vectors; that is, for vectors $\vec{a}$ and $\vec{b}$,

$$\sum_k a_k b_k = \vec{a} \cdot \vec{b} = \vec{a}^T \vec{b}. \tag{17}$$

In this manner, the sum of the elements in a single vector may be expressed as

$$\sum_k a_k = \vec{1}^T \vec{a}, \tag{18}$$

where $\vec{1}$ is a vector, the entries of which are each unity.

B. NORMAL MODES

The per-unit-length impedances and admittances from Sec. II may be separated into their real and imaginary components:

$$[Z_T] = [R_T] + j\omega\,[L_T] \tag{19a}$$

$$[Y_T] = [G_T] + j\omega\,[C_T] \tag{19b}$$

where $[R_T]$, $[L_T]$, $[G_T]$, and $[C_T]$ are the per-unit-length terminal domain resistance, inductance, conductance, and capacitance matrices (respectively) of the TL. All of these matrices are symmetric, real, and invertible. Substituting (19) into (8a) yields

$$\left(\begin{array}{c} [R_T][G_T] - \gamma_M^2\,[I] - \omega^2\,[L_T][C_T] \\ +j\omega\,([L_T][G_T] - [R_T][C_T]) \end{array} \right) \vec{V}_T = \vec{0} \tag{20}$$

The requirement that $[R_T] \rightarrow 0$ for TEM modes yields

$$\left(\gamma_M^2\,[L_T]^{-1} + j\omega\,[G_T] - \omega^2\,[C_T] \right) \vec{V}_T = \vec{0} \tag{21}$$

Invoking another requirement of TEM modes – that they must be supported inside a homogenous medium [1] – gives the requirement that $[G_T] = \frac{\sigma}{\epsilon}\,[C_T]$. Pre-multiplying by $[T_V]^T$ and invoking (9a) yields:

$$[T_V]^T \left(\gamma_M^2\,[L_T]^{-1} + j\omega\frac{\sigma}{\epsilon}\,[C_T] - \omega^2\,[C_T] \right) [T_V]\,\vec{V}_M = \vec{0} \tag{22}$$

In order for this system to be support a complete set of modes, $[L_T]^{-1}$ and $[C_T]$ must be simultaneously diagonalizable via the congruence transform by $[T_V]$. This occurs if and only if the matrix product $[L_T][C_T]$ is diagonalizable [27]. However, given the previously enforced TEM conditions, this statement

is equivalent to the existence of the modal propagation constants in (11a). Since the existence of modal propagation constants is generally taken as a pre-supposition to conducting modal analysis, it is assumed to hold true henceforth.

It may then be demonstrated that the eigenmodes of such a system are real. The similarity transformation $[T_V]^{-1}\,[L_T]\,[C_T]\,[T_V]$ can be factored into the product of two individual similarity transformations:

$$[T_V]^{-1}\,[L_T]\,[C_T]\,[T_V]$$
$$= \left([T_V]^{-1}\,[L_T]^{-1}\,[T_V] \right)^{-1} \left([T_V]^{-1}\,[C_T]\,[T_V] \right) \tag{23}$$

Since each of $[L_T]^{-1}$, $[C_T]$ is real and symmetric, it is guaranteed that each of these has eigenvalues. Since the eigenvalues of the matrix product are simply the product of these matrices' eigenvalues, it is the case that each of the eigenvalues of the left-hand side of (23) are real as well. Lastly, it is the case that if both the matrix product $[L_T]\,[C_T]$ and its eigenvalues are real, then its eigenvectors (i.e., $[T_V]$) may be expressed as entirely real as well – which is necessarily true for normal modes. A similar derivation demonstrates that $[T_I]$ may also be expressed as entirely real. These results stand in contraction to the foundational assumptions used in works such as [11], such that their conclusions – that modal properties cannot be determined in the TEM approximation – may not be substantiated.

C. POWER EQUIVALENCE

It may be demonstrated that the equality of total power between domains is a direct consequence of a particular constraint on the transformation matrices. Comparing (11a) with the transpose of (11b), and noting again that $[Z_T]$ and $[Y_T]$ must be symmetric, yields the constraint

$$[T_I]^T\,[T_V] = [I], \tag{24}$$

which is noted in [1]. Then, it may be proven that power is equivalent in both domains using (9a) and (9b), since:

$$\vec{I}_T^*\vec{V}_T = \vec{I}_M^*\,[T_I]^T\,[T_V]\,\vec{V}_M = \vec{I}_M^*\,\vec{V}_M \tag{25}$$

D. CURRENT EQUIVALENCE

Consider first a single excited mode, n, which is modelled with a two-conductor TL. The current magnitude for this mode is expressed, in accordance with the previous definitions, as I_{Mn}. While this is a single quantity, there are of course two currents present: one on each conductor. Let the magnitude of the current on one of the conductors be labelled $I_{M\,n}^{+z}$, and the magnitude of the current flowing in the opposite direction – that is, on the other conductor – be labelled $I_{M\,n}^{-z}$. Taking a sign to signify direction of propagation, the conservation of current (or charge) enforces that the currents sum to zero: $I_{M\,n}^{+z} + I_{M\,n}^{-z} = 0$, or equivalently, $I_{M\,n}^{+z} = -I_{M\,n}^{-z}$.

Next, consider a TL with more than two conductors, as described in the terminal domain. It is certain that the conservation of current specifies that the sum of the currents on all conductors must be zero, and also therefore,

that the sums of the magnitudes of the individual positive- and negative-directed currents must be equal (noting that *magnitude* does not refer to magnitude of the vector):

$$\sum_n I_{Tn} = 0 \Rightarrow \sum_n I_{Tn}^{+z} = -\sum_n I_{Tn}^{-z} \qquad (26)$$

where $\vec{I}_T^{+z}$ and $\vec{I}_T^{-z}$ are the sets of positively and negatively-directed currents, respectively. Since it has been established that TL modes are normal, it must be the case (for TEM modes: strictly; and for quasi-TEM modes: approximately) that although these currents are solved as complex quantities, they may only only possess given phases θ or $\theta \pm 180°$, which are used to assign membership to the $+z$ or $-z$ sets.

The same relations may be applied in the modal domain. The conservation of currents still enforces that the currents sum to zero, such that:

$$\sum_n I_{Mn} = 0 \Rightarrow \sum_n I_{Mn}^{+z} = -\sum_n I_{Mn}^{-z} \qquad (27)$$

The postulate of equality of total currents simply states that the sums of the modal- and terminal-domain currents in each directed set are equal: i.e.,

$$\sum_n I_{Mn}^{+z} = \sum_n I_{Tn}^{+z}, \quad \sum_n I_{Mn}^{-z} = \sum_n I_{Tn}^{-z} \qquad (28)$$

These relations are then inserted into the MTL formalisms of Sec. II. The set of total currents on all conductors may be expressed as the vector:

$$\vec{I}_T = \vec{I}_T^{+z} + \vec{I}_T^{-z} \qquad (29)$$

where $\vec{I}_T^{-z}$ will then contain an entry of zero wherever $\vec{I}_T^{+z}$ has a nonzero entry, and vice-versa, such that all vectors have the same length (which is the number of conductors in the TL). It is known from (9b) that the distribution of terminal-domain currents is dictated by the transformation matrix $[T_I]$ – that is, if a single mode is excited, the currents on each conductor are specified by the corresponding column of $[T_I]$. Let the transformation matrix then be separated into two new matrices – one, labelled $\left[T_I^{+z}\right]$, consisting of the magnitudes of the components related to the set of currents $\vec{I}_T^{+z}$, and another labelled $\left[T_I^{-z}\right]$ consisting of the magnitudes of the components related to the set of currents $\vec{I}_T^{-z}$. Then,

$$[T_I] = \left[T_I^{+z}\right] - \left[T_I^{-z}\right] \qquad (30a)$$
$$\vec{I}_T^{-z} = \left[T_I^{-z}\right]\vec{I}_M \qquad (30b)$$
$$\vec{I}_T^{+z} = \left[T_I^{+z}\right]\vec{I}_M \qquad (30c)$$

Then, consider the case of a single excited mode n. Applying the expression form of (18), the postulate (28) then may be expressed as:

$$I_{Mn}^{-z} = \vec{1}^T \vec{I}_T^{-z}\Big|_n \qquad (31a)$$

$$I_{Mn}^{+z} = \vec{1}^T \vec{I}_T^{+z}\Big|_n \qquad (31b)$$

Invoking (15b) and (30b) allows the previous expressions to be expanded to

$$I_{Mn}^{-z} = \vec{1}^T \left[T_I^{-z}\right]\vec{\delta}_n I_{Mn}^{-z} \qquad (32a)$$
$$I_{Mn}^{+z} = \vec{1}^T \left[T_I^{+z}\right]\vec{\delta}_n I_{Mn}^{+z} \qquad (32b)$$

The scalars I_{Mn}^{-z} and I_{Mn}^{+z} can then be cancelled to yield the expressions:

$$1 = \vec{1}^T \left[T_I^{-z}\right]\vec{\delta}_n \qquad (33a)$$
$$1 = \vec{1}^T \left[T_I^{+z}\right]\vec{\delta}_n \qquad (33b)$$

which simply imply that the sum of each column n in $\left[T_I^{-z}\right]$ and $\left[T_I^{+z}\right]$ must be equal to unity.

E. PROPOSED SOLUTION PROCESS

A procedure for the determination of the transformation matrices $[T_V]$ and $[T_I]$ may then be developed by utilizing the equality of power (24) and the equality of currents (33). Specifically, the scaling factor of $[T_I]$ may be determined through the use of the equality of current, with the equality of power being used to relate $[T_V]$ to $[T_I]$. Let the scaled transformation matrix $[T_I]$ be defined as:

$$[T_I]_{\text{scaled}} = [T_I]_{\text{unscaled}} \cdot [g] \qquad (34)$$

where $[g]$ is the matrix of scaling factors determined via the application of the equality of total currents, which will be defined shortly. Firstly, the unscaled transformation matrix may be determined using (11b) via an eigenmode process in which $[T_I]_{\text{unscaled}}$ are returned as eigenvectors. If $[T_V]_{\text{unscaled}}$ is solved from (11a), $[T_I]_{\text{unscaled}}$ may be determined through the application of (24).

Secondly, the equality of current is applied to $[T_I]_{\text{unscaled}}$, where a minor technicality adds some complication: specifically, that the currents excited on the reference conductor are typically not included in either the set of currents $\vec{I}_T$, nor the transformation matrix $[T_I]$. However, it will be the case that either this current is positive, negative, or zero. In the case that it is positive, it would be found that the sum of $\left[T_I^{-z}\right]\vec{\delta}_n$ would be smaller than that of $\left[T_I^{+z}\right]\vec{\delta}_n$. In the case that it is negative, it would be found that the sum of $\left[T_I^{+z}\right]\vec{\delta}_n$ would be larger than that of $\left[T_I^{+z}\right]\vec{\delta}_n$. If it were zero, the sums of the two vectors would be equal. Therefore, for the equivalence of current to hold, at least one of the sums is required to be equal to one, with the other being less than or equal to one. The columns of the two matrices $\left[T_I^{+z}\right]$ and $\left[T_I^{-z}\right]$ are then compared, and the one with the larger sum is selected. The corresponding value of $[g]$ (which is diagonal) is then the inverse of this sum, in order to normalize the total currents, i.e.:

$$g_{nn} = \max\left[\left(\vec{1}^T \left[T_I^{-z}\right]\vec{\delta}_n\right), \left(\vec{1}^T \left[T_I^{+z}\right]\vec{\delta}_n\right)\right]^{-1} \qquad (35)$$

Lastly, the equality of power (24) is used to obtain $[T_V]_{\text{scaled}}$ from $[T_I]_{\text{unscaled}}$ and $[g]$, that is:

$$[T_V]_{\text{scaled}} = \left([g][T_I]_{\text{unscaled}}^T\right)^{-1} \qquad (36)$$

A proposed algorithm for scaling the transformation matrices with the proposed process and associated discussion are given in Appendix A.

Of course, the sorting of terminal domain currents into either of $\vec{I}_T^{-z}$ or $\vec{I}_T^{+z}$ possesses some inherent ambiguity: the sets are simply distinguished by sign, and may easily be reversed when applied in (30a). This results in an arbitrary sign being applied to the entire column of $[T_I]$, which may be physically understood as an arbitrary choice of conductors supporting negative current and voltage. For example, in a symmetric three-wire system, the differential mode will have oppositely directed currents; but the choice of conductor carrying the "negative" current is arbitrary; the mode's properties do not change if the signs of the currents are reversed.

IV. EXAMPLES

This section will examine two realistic examples of determining a MTL's modal properties. Ansys HFSS was used to extract the per-unit-length inductance and capacitance matrices in the terminal domain, as well as determine the propagation constants and characteristic impedances in the modal domain (chosen since these are the only available modal-domain properties), all computed at a frequency of 1 GHz. Since HFSS is understood to correctly compute the modal quantities from field data (using the built-in modal solver in the Driven Terminal simulation type), the results it produces may be considered physically accurate. The convergence criteria for the HFSS simulations were chosen to be extremely strict, in order to rigorously verify the proposed method. These criteria enforced a minimum of 20 converged passes with a convergence $\Delta |S|$ of 0.0001 and $\Delta \angle S$ of 0.1°. The validity and effectiveness of the proposed process is established by the corroboration of the HFSS modal values, given only the known terminal values.

A. CONDUCTOR-BACKED COPLANAR STRIPLINE

This conductor-backed coplanar stripline (CBCPS) MTL (which is equivalent to a pair of coupled microstrips), detailed in Fig. 1, consists of three rectangular solid copper conductors of thickness $t = 35 \mu m$ (bulk conductivity $\sigma = 58$ MS/m) on a Rogers RO-3003 substrate ($\epsilon_r = 3.0$, $\tan \delta = 0.0013$)
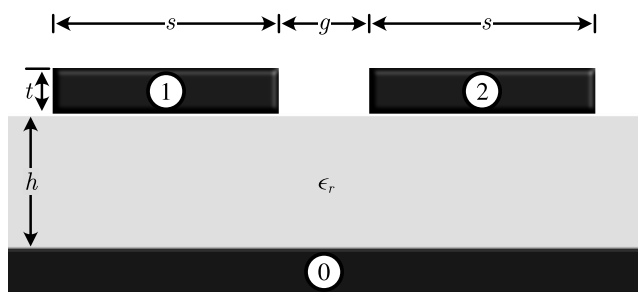

FIGURE 1. Physical arrangement and properties of the conductor-backed coplanar stripline (CBCPS). Conductor 0 and the dielectric extend much further along the horizontal axis than shown (30 mm).

with thickness $h = 1.524$ mm. The dielectric and conductor 0 (taken to be the reference conductor) have a total width of 30 mm, which is not shown to scale in Fig. 1. The upper conductors 1 and 2 are symmetric with widths $s = 1.7$ mm and spacing $g = 0.4$ mm. The terminal-domain per-unit-length TL parameter matrices are 2×2 in size and extracted in HFSS as

$$[R_T] = \begin{bmatrix} 5.6364 & 0.1963 \\ 0.1963 & 5.6364 \end{bmatrix} \Omega/m$$

$$[L_T] = \begin{bmatrix} 0.3827 & 0.1452 \\ 0.1452 & 0.3827 \end{bmatrix} \mu H/m$$

$$[G_T] = \begin{bmatrix} 4.7759 & -1.0613 \\ -1.0613 & 4.7759 \end{bmatrix} mS/m$$

$$[C_T] = \begin{bmatrix} 73.1102 & -21.6745 \\ -21.6745 & 73.1102 \end{bmatrix} pF/m \quad (37)$$

which are used to solve the terminal-domain voltage propagation constants and characteristic impedances:

$$[\gamma_{VT}] = \begin{bmatrix} 0.0582+j31.2759 & -0.0107+j1.4645 \\ -0.0107+j1.4645 & 0.0582+j31.2759 \end{bmatrix} rad/m$$

$$[Z_{cT}] = \begin{bmatrix} 75.6818-j0.0488 & 25.6249+j0.0179 \\ 25.6249+j0.0179 & 75.6818-j0.0488 \end{bmatrix} \Omega$$
$$(38)$$

Using (3a) in (11a) yields the modal propagation constants and characteristic impedances:

$$[\gamma_M] = diag \begin{bmatrix} 0.0689 + j29.8114 \\ 0.0476 + j32.7403 \end{bmatrix} rad/m$$

$$[Z_{cM}] = diag \begin{bmatrix} 50.0570 - j0.0667 \\ 101.3070 - 0.0309 \end{bmatrix} \Omega \quad (39)$$

along with the (unscaled) transformation matrices (where *diag* indicates the entries on the lead diagonal of a diagonal matrix, in which the off-diagonal entries are zero):

$$[T_V]_{\text{unscaled}} = [T_I]_{\text{unscaled}} = \frac{1}{\sqrt{2}} \begin{bmatrix} -1 & 1 \\ 1 & 1 \end{bmatrix} \quad (40)$$

which are the well-known mode definitions of the even and odd modes of the system [1], [7], [10], [28]. HFSS gives the modal propagation constants and characteristic impedances:

$$[\gamma_M]_{HFSS} = diag \begin{bmatrix} 0.0733 + j29.8120 \\ 0.0458 + j32.7410 \end{bmatrix} rad/m$$

$$[Z_{cM}]_{HFSS} = diag \begin{bmatrix} 100.2400 - j0.1369 \\ 50.3630 - j0.0124 \end{bmatrix} \Omega \quad (41)$$

where it may be confirmed that the modal propagation constants are very similar (percent differences of less than 0.01% between HFSS direct eigenmode simulation and the data computed from the terminal-domain values). The characteristic impedances appear to have values that are interchanged relative to those predicted by the typical mode definitions (40): a coincidence for this system that, nonetheless, illustrates that these mode definitions – based on unscaled transformation matrices – are expectedly in rather *strong disagreement* with HFSS.

Investigating the mode definitions in more detail, it can be noted that the unscaled matrices satisfy the equality of total power (24). However; the current transformation matrix $[T_I]$ does not satisfy the equality of total current (33), which is integral to the scaling process proposed in this work. Scaling the mode definitions through the application of this proposed constraint yields the matrices

$$[g] = diag \begin{bmatrix} \sqrt{2} \\ \sqrt{2} \\ 2 \end{bmatrix}$$

$$[T_V]_{\text{scaled}} = \begin{bmatrix} -0.5 & 1 \\ 0.5 & 1 \end{bmatrix}$$

$$[T_I]_{\text{scaled}} = \begin{bmatrix} -1 & 0.5 \\ 1 & 0.5 \end{bmatrix} \tag{42}$$

which have also been noted in the recent literature [22], [29]. Using these definitions in (12) gives:

$$[Z_{cM}] = diag \begin{bmatrix} 100.1140 - j0.1334 \\ 50.6534 - j0.0154 \end{bmatrix} \Omega \tag{43}$$

which are now in good agreement with percent differences of 0.13% and 0.57%, for the odd and even mode, respectively, to the modal values given by HFSS (41) as compared with those in (39). The dramatic improvement in accuracy seen in this case validates the proposed process, while the minor remaining discrepancies are limited to firstly the TEM approximation, and secondly errors introduced through numerical processing.

B. ASYMMETRIC SHIELDED CONDUCTOR-BACKED COPLANAR WAVEGUIDE

This MTL, which exhibits physical asymmetry along both transverse axes, consists of five rectangular solid copper conductors of thickness $t = 35$ μm (bulk conductivity $\sigma = 58$ MS/m) on a Rogers RO-3010 substrate ($\epsilon_r = 11.2$, $\tan \delta = 0.0035$) with thickness $h_l = 1.270$ mm. The width of the simulation domain is 10 mm. The various other geometric parameters detailed in Fig. 2 are $s_1 = 1.8$ mm, $s_2 = 3.1$ mm, $s_3 = 0.8$ mm, $g_1 = 2.4$ mm, $g_2 = 1.3$ mm, $g_3 = 0.6$ mm, $h_u = 20$ mm. The domain is bounded on the sides with perfect magnetic conductors (PMCs). The terminal-domain per-unit-length TL parameter matrices are then 4×4 in size, with

$$[R_T]$$
$$= \begin{bmatrix} 5.7410 & 0.6158 & 0.4285 & 1.3669 \\ 0.6158 & 3.4829 & 0.7249 & 1.3292 \\ 0.4285 & 0.7249 & 9.7946 & 1.2298 \\ 1.3669 & 1.3292 & 1.2298 & 2.6073 \end{bmatrix} \Omega/m \tag{44a}$$

$$[L_T]$$
$$= \begin{bmatrix} 0.4871 & 0.0589 & 0.0375 & 0.1613 \\ 0.0589 & 0.2844 & 0.0969 & 0.1613 \\ 0.0375 & 0.0969 & 0.5967 & 0.1612 \\ 0.1613 & 0.1613 & 0.1612 & 2.6769 \end{bmatrix} \mu H/m \tag{44b}$$
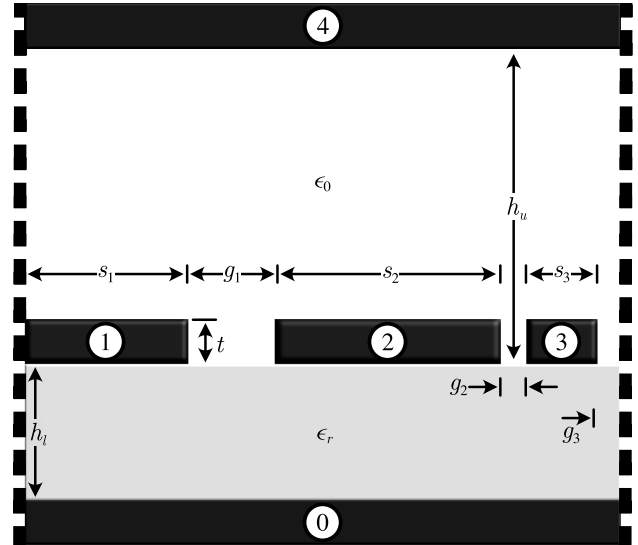

FIGURE 2. Physical arrangement and properties of the shielded conductor-backed coplanar waveguide. The vertical dashed lines on the sides indicate perfect-magnetic-conductor (PMC) boundary conditions.

$$[G_T]$$
$$= \begin{bmatrix} 4.1004 & -0.0920 & -0.0183 & -0.0004 \\ -0.0920 & 7.3164 & -0.2782 & -0.0005 \\ -0.0183 & -0.2782 & 3.0389 & -0.0016 \\ -0.0004 & -0.0005 & -0.0016 & 0.0001 \end{bmatrix} mS/m \tag{44c}$$

$$[C_T]$$
$$= \begin{bmatrix} 192.9900 & -6.9559 & -0.7568 & -1.0823 \\ -6.9559 & 346.2750 & -17.4292 & -1.8796 \\ -0.7568 & -17.4292 & 145.6230 & -0.7419 \\ -1.0823 & -1.8796 & -0.7419 & 4.4208 \end{bmatrix} pF/m \tag{44d}$$

which are used to solve the terminal-domain voltage propagation constants and characteristic impedances:

$$[\gamma_{VT}]$$
$$= \begin{bmatrix} 0.1597 & 0.0139 & 0.0033 & 0.0002 \\ 0.0078 & 0.1646 & 0.0051 & 0.0001 \\ 0.0050 & 0.0110 & 0.1733 & 0.0002 \\ 0.0394 & 0.0680 & 0.0244 & 0.0012 \end{bmatrix}$$
$$+ j \begin{bmatrix} 60.5802 & 5.1182 & 1.1871 & 0.0215 \\ 2.9128 & 61.2832 & 2.9531 & 0.0191 \\ 1.7954 & 7.4158 & 57.7375 & 0.0214 \\ 12.1225 & 20.9886 & 8.3301 & 21.0419 \end{bmatrix} rad/m \tag{45a}$$

$$[Z_{cT}]$$
$$= \begin{bmatrix} 50.1787 & 3.5449 & 2.0584 & 14.9098 \\ 3.5449 & 28.6587 & 6.7518 & 14.8751 \\ 2.0584 & 6.7518 & 63.9974 & 14.8850 \\ 14.9098 & 14.8751 & 14.8850 & 770.0090 \end{bmatrix}$$

$$+j \begin{bmatrix} 0.0380 & 0.0041 & 0.0020 & 0.0169 \\ 0.0041 & 0.0204 & 0.0107 & 0.0177 \\ 0.0020 & 0.0107 & 0.0224 & 0.0224 \\ 0.0169 & 0.0177 & 0.0215 & 0.0229 \end{bmatrix} \Omega$$

(45b)

Using (3a) in (11a) yields the modal propagation constants and characteristic impedances (in vector form):

$$[\gamma_M] = diag \begin{bmatrix} 0.0014 + j21.0236 \\ 0.1610 + j54.2975 \\ 0.1570 + j58.2701 \\ 0.1795 + j67.0516 \end{bmatrix} rad/m$$

$$[Z_{cM}] = diag \begin{bmatrix} 661.2290 - j0.1385 \\ 38.7598 + j0.0520 \\ 48.6598 - j0.0094 \\ 53.0236 + j0.0383 \end{bmatrix} \Omega$$

(46)

along with the (unscaled) transformation matrices:

$$[T_V]_{unscaled}$$
$$= \begin{bmatrix} -0.0005 & 0.2043 & 0.8007 & 0.5056 \\ -0.0004 & -0.4522 & -0.2335 & 0.5187 \\ -0.0005 & 0.8682 & -0.5516 & 0.5115 \\ 0.9999 & 0.0069 & 0.0056 & 0.4624 \end{bmatrix}$$
$$+j \begin{bmatrix} 0.0000 & -0.0015 & 0.0005 & 0.0001 \\ 0.0000 & 0.006 & -0.0011 & 0.0000 \\ 0.0000 & 0.008 & 0.0012 & -0.0005 \\ 0.0000 & 0.0003 & -0.0002 & 0.0003 \end{bmatrix}$$

(47a)

$$[T_I]_{unscaled}$$
$$= \begin{bmatrix} -0.2314 & 0.1880 & 0.8215 & 0.4624 \\ -0.3967 & -0.7764 & -0.4031 & 0.8263 \\ -0.1591 & 0.6015 & -0.4033 & 0.3216 \\ 0.8739 & 0.0000 & 0.0000 & 0.0007 \end{bmatrix}$$
$$+j \begin{bmatrix} -0.0001 & -0.0011 & -0.0002 & 0.0001 \\ -0.0002 & 0.0006 & 0.0017 & 0.0000 \\ -0.0002 & 0.0011 & 0.0013 & -0.0004 \\ -0.0001 & 0.0000 & 0.0000 & 0.0000 \end{bmatrix}$$

(47b)

It may be noted that although $[T_V]_{unscaled}$ and $[T_I]_{unscaled}$ are complex matrices, the mode definitions still imply that the characteristic modes are *approximately* normal, as previously indicated should be the case. HFSS gives the modal propagation constants and characteristic impedances:

$$[\gamma_M]_{HFSS} = diag \begin{bmatrix} 0.0014 + j21.0240 \\ 0.1621 + j54.3010 \\ 0.1576 + j58.2720 \\ 0.1799 + j67.0550 \end{bmatrix} rad/m$$

$$[Z_{cM}]_{HFSS} = diag \begin{bmatrix} 756.1500 - j0.0521 \\ 57.6910 + j0.1264 \\ 71.6100 - j0.0361 \\ 16.8950 + j0.0133 \end{bmatrix} \Omega$$

(48)

where it may be confirmed that the modal propagation constants are very similar (percent differences of less than 0.01%

in both cases), while the characteristic impedances differ greatly from those predicted in (46) through application of (12). Scaling the transformation matrices yields:

$$[g] = diag \begin{bmatrix} 1.1443 + j0.0001 \\ -1.2666 - j0.0009 \\ -1.2173 - j0.0003 \\ 0.6207 + j0.0001 \end{bmatrix}$$

$$[T_V]_{scaled} = \begin{bmatrix} -0.0005 & -0.1769 & -0.6751 & 0.9847 \\ -0.0004 & 0.3916 & 0.1969 & 1.0102 \\ -0.0005 & -0.7518 & 0.4651 & 0.9962 \\ 0.9996 & -0.0057 & -0.0048 & 0.9006 \end{bmatrix}$$

$$[T_I]_{scaled} = \begin{bmatrix} -0.2648 & -0.2381 & -1.0000 & 0.2871 \\ -0.4542 & 0.9834 & 0.4906 & 0.5129 \\ -0.1818 & -0.7619 & 0.4909 & 0.1996 \\ 1.0000 & 0.0000 & 0.0000 & 0.0004 \end{bmatrix}$$

(49)

Using these definitions to compute the modal impedances yields:

$$[Z_{cM}] = diag \begin{bmatrix} 756.9000 - j0.0452 \\ 56.6762 + j0.0177 \\ 70.2499 + j0.0474 \\ 16.8991 - j0.0130 \end{bmatrix} \Omega$$

(50)

which are now in good agreement (percent differences of 0.01%, 1.77%, 1.92%, 0.02% to the modal values given by HFSS (48) as compared with those in (46). It may be noted that the two modes with a roughly even distribution of fields in both dielectrics are those two that exhibit the highest error. This is unsurprising, since the contrast between relative permittivities of 1.0 and 11.2 is very high, and these modes are stretching the limitations of the TEM approximation, thereby incurring the most error when using processes derived for strictly TEM modes. This example illustrates, however, the robustness of the proposed process even in such extreme cases.

C. SUMMARY AND CONTRADICTIONS WITH OTHER PROCESSES

The results given in these examples demonstrate that the proposed process achieves agreement with computed field quantities. Moreover, the invocation of physical arguments such as the equality of total currents implies that this process is uniquely required to achieve that agreement – and that therefore, other methods should result in inherent contradictions. The two predominant methods of scaling are given in (13) and (14), which are examined for inconsistencies with the field solutions.

It may be readily observed that (13) conflicts with the equality of total power (24), such that any diagonal matrix $[D]$ (13) which is not identity represents a system in which total power is dependent on the chosen basis of voltages and currents: a physical contradiction. Therefore, (13) is superseded by (24).

Self-normalization of the current or voltage eigenvectors as described in (14) is typically used by most eigenmode

solvers; indeed, this can be seen to be the case in the unscaled mode definitions of (40) and (47). Since it was demonstrated that these do not produce results in agreement with at least the field solutions studied previously, this scaling process may also be discounted as invalid. Quantitative results of these conclusions are provided in Table 1, which details comparisons of modal characteristic impedance values computed via self-normalization of eigenvectors (as well as the less commonly used case of solving the eigenmodes of the terminal-domain characteristic impedance matrix [30] given in Appendix B) with the values computed from HFSS.

TABLE 1. Comparison of percent differences in modal characteristic impedances produced by various computational methods with respect to data produced by HFSS.

Method	Example 1	Example 2
Self-Normalization [1], [7]	66.78%, 67.18%	13.39%, 39.26%, 38.16%, 103.34%
Diagonalization of $[Z_{cT}]$ [30]	66.67%, 66.67%	1.94%, 9.44%, 14.51%, 45.53%
Proposed Method	< 0.01% both cases	0.01%, 1.77%, 1.92%, 0.02%

V. EXPERIMENTAL VALIDATION

A. EXPERIMENT MODELLING AND SETUP

The modal characteristic impedance values predicted by the proposed scaling process, as well as the simulations, may also be confirmed via experiment, which also illustrates the value of knowing the modal impedances when interfacing MTLs with other TLs. Modal characteristic impedances of two different CBCPS MTLs are confirmed though the excitation of each of their two propagation modes. Specifically, the proposed setup consists of a length of CBCPS, connected on either end to a feeding two-conductor TL. The equivalent-circuit models of two such designs are shown in Figs. 3 and 4. The validation occurs in observing the scattering of the total system: since the impedances of the two-conductor feeding TLs are well known as well as determinable, and if the feed lines excite predominantly a single mode of the MTL, then the observed scattering parameters should correspond to particular modal impedances. For example, the return losses should be low (at least 20 dB over a wide bandwidth) for a matched modal impedance, and high for an unmatched case, both with a predictable frequency response corresponding to the MTL lengths.

In order to excite each mode of the CBCPS MTLs, two different feed TLs are designed. Since the characteristic modes are simply the odd and even modes (described by the mode definitions in (42)), a CPS TL may be used to excite the odd mode, and a microstrip (MS) TL may be used to excite the even mode. The impedances of these lines are chosen to be 100 Ω and 50 Ω, respectively, such that the design in Sec. IV-A should represent the matched case for both even and odd modes. Designed on the same RO-3003 substrate, the MS has a width of 3.8 mm, and the CPS has a strip width $s = 1.4$ mm and spacing $g = 0.2$ mm. The second
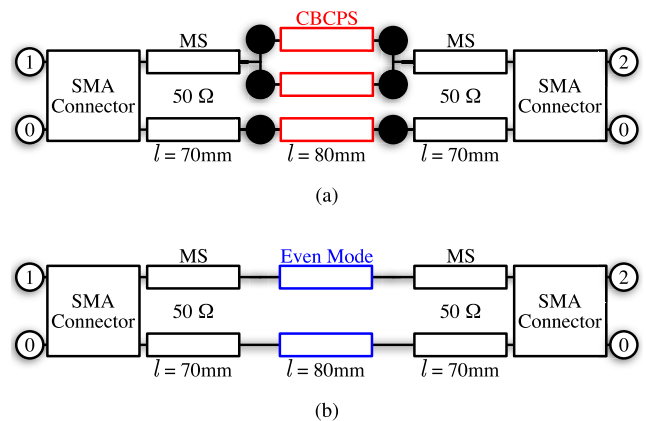

FIGURE 3. Equivalent-circuit models of the experimental even-mode structures: (a) the terminal domain layout, and (b) the equivalent modal-domain circuit.
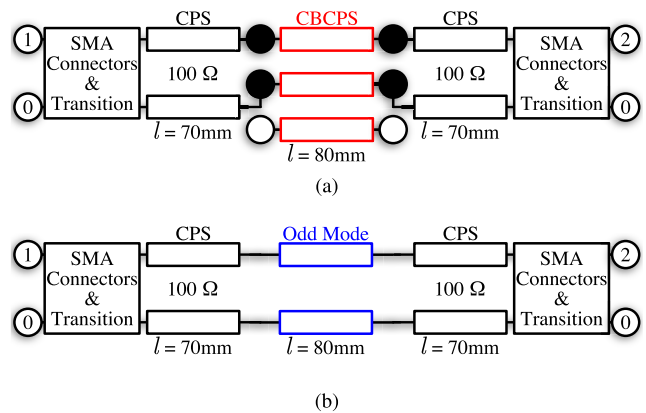

FIGURE 4. Equivalent-circuit models of the experimental odd-mode structures: (a) the terminal domain layout, and (b) the equivalent modal-domain circuit.

CBCPS, representing the mismatched case, is designed on an identical substrate with geometrical parameters $s = 0.23$ mm and $g = 0.55$ mm, for which the proposed analytical process predicts impedances of roughly 200 Ω and 100 Ω for the odd and even modes, respectively.

The connections between the two-conductor feed lines and the MTLs are also detailed in Figs. 3 and 4. The even mode is excited in the MTLs through shorting the MS to both upper-layer conductors, such that they possess the same voltage and the currents are equally divided between them. The conductor backing of both the feed and CBCPS are connected directly together. The odd-mode feed connects each conductor of the CPS directly to each of the upper-layer conductors of the CBCPS, while the conductor backing of the CBCPS is left floating with no connection. This ensures that the currents and voltages are equal and opposite on the upper-layer conductors.

Both feed line types are connected to a Vector Network Analyzer (VNA) via SMA connectors and coaxial

phase-stable measurement cables. The MS TL is directly connected to one SMA connector, while the two conductors of the CPS are split and individually connected each to a SMA connector (the details of this transition are given in Appendix C), such that the odd mode must be differentially excited. These transition sections are included in the modal-domain equivalent-circuit models of Figs. 3b and 4b, and their computed scattering parameters are given by the dotted curves in Figs. 5 (the matched case) and 6 (the mismatched case). The entire system of connectors, transition sections, feed lines, and CBCPS sections are then simulated in ANSYS HFSS, the layouts of which are shown in Figs. 7 and 8, and the results are given in Figs. 5 and 6 via the dashed curves.
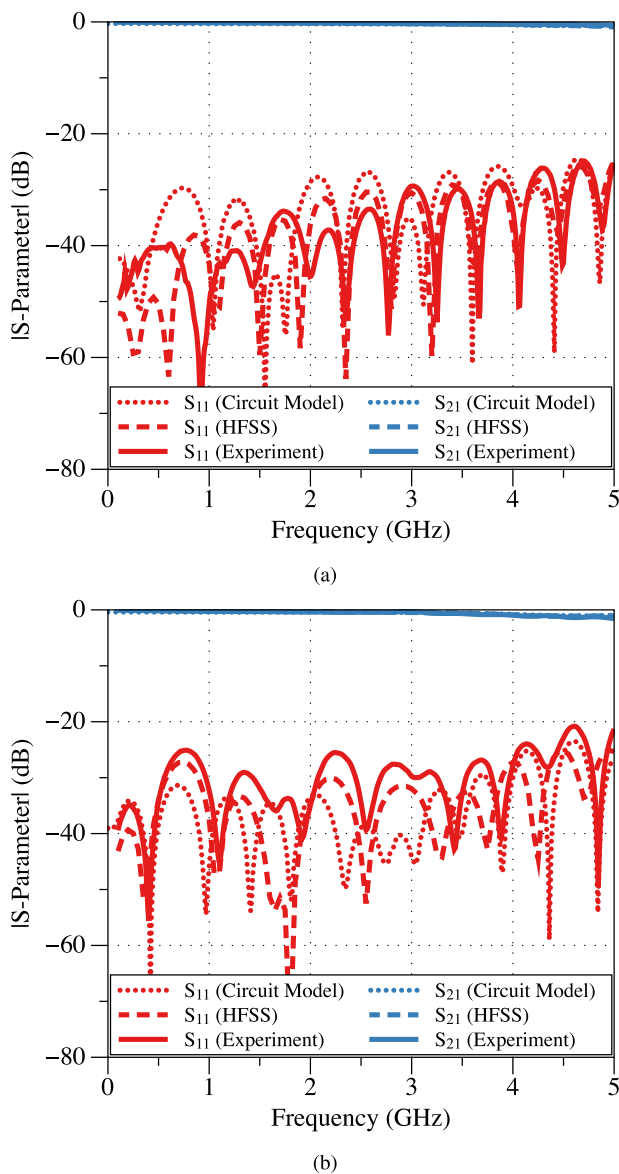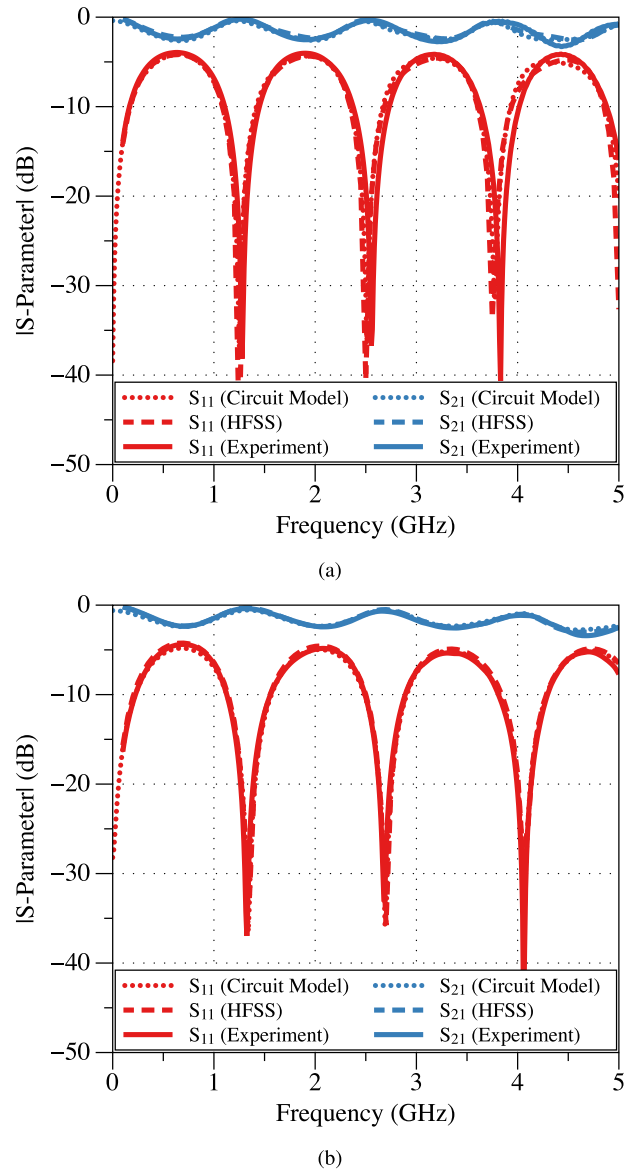

FIGURE 5. Scattering parameters of the matched MTL (dotted: equivalent-circuit model, dashed: HFSS simulation, solid: experimental data, red curves: S_{11}, blue curves: S_{21}): (a) even-mode MS excitation, (b) odd-mode CPS excitation.

FIGURE 6. Scattering parameters of the mismatched MTL (dotted: equivalent-circuit model, dashed: HFSS simulation, solid: experimental data, red curves: S_{11}, blue curves: S_{21}): (a) even-mode MS excitation, (b) odd-mode CPS excitation.
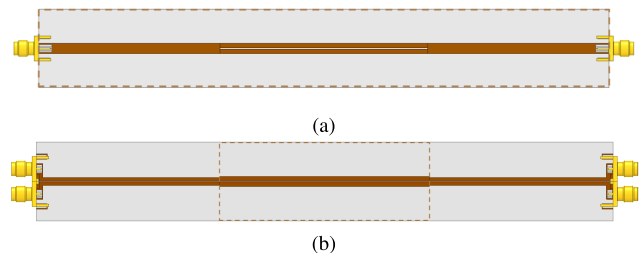

FIGURE 7. Simulation models of the matched CBCPS structures: (a) even-mode MS excitation, (b) odd-mode CPS excitation, where the dashed lines indicate the location of the conductor backing.

The devices are then fabricated using a LPKF U3 laser-based milling machine, which is calibrated to achieve
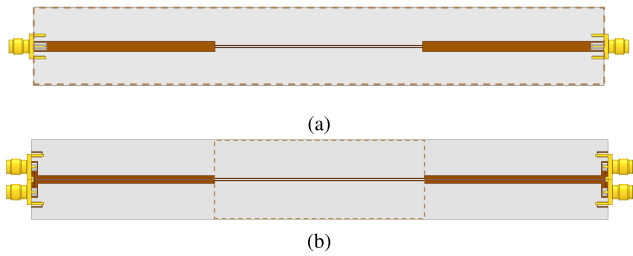
FIGURE 8. Simulation models of the mismatched CBCPS structures: (a) even-mode MS excitation, (b) odd-mode CPS excitation, where the dashed lines indicate the location of the conductor backing.

a positional accuracy of at least 10 μm across each PCB. Shown in Figs. 9, the fabrications are visually inspected and the positional inaccuracies are estimated to be at most 2 μm in the regions of interest; particularly, the 50 μm gaps in the CPS feed transitions sections.
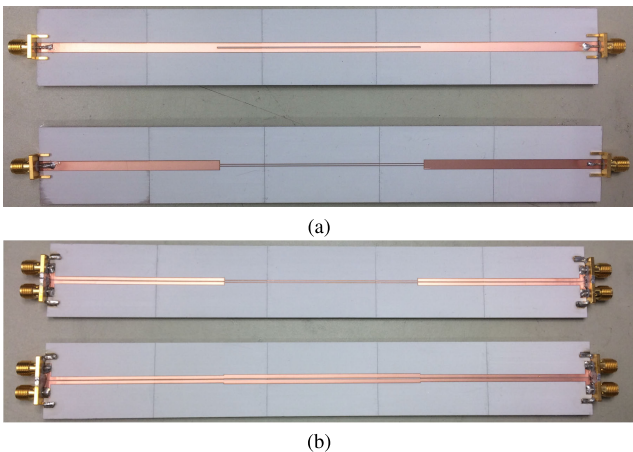

FIGURE 9. Fabricated CBCPS structures: (a) even-mode MS excitation, (b) odd-mode CPS excitation.

The devices are connected to a four-port VNA, as shown in Fig. 10, where a styrofoam base has been used to support the structures and mitigate parasitic coupling with any metallic features in the table below. The measured scattering parameters are given in Figs. 5 and 6 via the solid curves, where the odd-mode scattering parameters are obtained via modal transformation from the four-port terminal-domain data as described in Appendix D.

B. DISCUSSION ON RESULTS

Comparing the results of the two simulation models and experimental data (Figs. 5 and 6), it may be observed that the measured data are in close agreement with the simulation data, indicating the modal-domain circuit models of Figs. 3b and 4b are valid, high-fidelity representations of the corresponding terminal-domain circuit models of Figs. 3a and 4a. With the return loss of the matched cases better than 20 dB over the very large bandwidth of 0.1 to 5.0 GHz, it may be concluded that, indeed, the MTL is well matched to 50 and
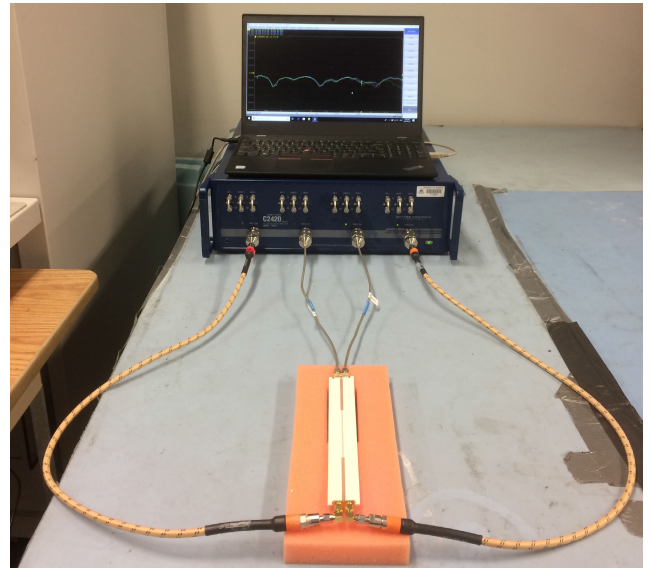

FIGURE 10. Experimental setup of the odd-mode-excited CBCPS test structure connected to a four-port VNA.

100 Ω for the even and odd modes, respectively, which must then be its modal impedance values, as predicted by the proposed scaling process. It is critical to note that this stands in stark contrast to the modal impedances computed with the common (unscaled) mode definitions (40), which predict that these MTL sections would always be mismatched (these data are provided in Appendix E) – lending further credibility to the proposed process. Additionally, the scattering parameters of the mismatched cases align readily with the those predicted by the equivalent-circuit model, indicating that these predicted values are indeed those observed in experiment.

The finite – but small – S_{11} ripples observed in Figs. 5 below -20 dB are attributed to impedance mismatches between the MTL and the feed lines. These minor mismatches arise from the fact that the modal impedances of the MTL sections (with values given in (41) are not identical to those of the feed lines. The MTL modal impedance are not exactly 50 and 100 Ω due to the consideration of a minimum geometrical step size of 0.01 mm in simulation, which is also likely close to the actual fabrication error of the laser milling system.

Since both modes are validated, both in the matched and mismatched cases, it has been experimentally established that a) the modal characteristic impedances of the MTLs are not arbitrary; their values do affect matching with standard two-conductor TLs, and furthermore, b) these modal values may be successfully predicted by scaling of the mode definitions using the proposed process.

To further establish that the data in Figs. 5a and 5b do indeed represent the matched case, and that other mismatched cases may be predicted via their modal impedance values, additional parametric sweeps of the CBCPS modal domain impedances and associated scattering parameters are presented in Appendix E.

VI. CONCLUSION

It has been demonstrated that various properties of the characteristic modes of MTLs may be predicted analytically through the application of the equality of total currents to the modal-terminal-domain transformation process. It was shown that the characteristic modes are normal, and that as a result, physically-based scaling factors for a MTL's voltage and current transformation matrices may be extracted using the equivalence of total current between terminal and modal domains. Various examples further demonstrated the use and accuracy of the proposed scaling process, through comparison with HFSS simulations, and finally validated experimentally, where it is shown that predictions made with common, well-accepted definitions fail. The determination of the properties of TL modes may find meaningful applications in matching MTLs of differing geometric configurations, as well as in areas such as electromagnetic compatibility or mutual coupling analysis; and signal and power integrity in printed-circuit-board environments and power system circuits. It also allows the for the analytical computation of Bloch modal properties for periodic MTL-based structures such as transmission-line metamaterials, which presently cannot be directly computed from circuit models.

.

APPENDIX A PROPOSED SCALING ALGORITHM

Obtaining the sum of each of the (non-reference-conductor) components of the columns of $[T_I]$ will yield two quantities: if these values are equal, then it can be stated conclusively that the current component on the reference conductor is zero, and that the value of $g_{I nn}$ is simply the inverse of either the positive or negative sum. If the two sums do not have the same magnitude, then the larger sum is the correct value (with the difference being the current component on the reference conductor), the inverse of which is $g_{I nn}$. With this knowledge, the pseudocode Alg. 1 is proposed, where all scalar or matrix values are assumed to be of a complex, floating-point type, unless they are indices (in which case they are integer values).

This algorithm has an outermost loop which iterates over each column. The inner loop has four main processes: in order of operation, the positive and negative sums are computed, and the larger sum is selected and evaluated. The column's g is then multiplied by the inverse of the sum. Lastly, once the complete $[g]$ matrix has been calculated for all columns, the scaled $[T_I]$ can be calculated, and utilizing the power equality, $[T_V]$ is calculated directly from this. Both scaled matrices are then returned.

APPENDIX B CHARACTERISTIC IMPEDANCE VALUES OBTAINED FROM DIAGONALIZATION OF $[Z_{cT}]$

Some works such as [30] indicate that the modal characteristic impedance matrix $[Z_{cM}]$ may be calculated as the eigenvalues of the terminal-domain characteristic impedance matrix $[Z_{cT}]$ (there appears to be no theoretical validation for this statement). Using this process, the modal characteristic impedance matrices from the examples in section IV-A were

---

Algorithm 1 $[T_V]$ and $[T_I]$ Scaling Procedure

1: **procedure** ScaleTvTi($[T_V]$, $[T_I]$)
2:　　$[g] \leftarrow [I]$　　　　　　▷ Initialize $[g]$ with identity
3:　　**for** Each Column n **do**
4:　　　　$NegSum \leftarrow 0$
5:　　　　$PosSum \leftarrow 0$
6:　　　　$LargerSum \leftarrow 0$
7:　　　　**for** Each Row k **do**
8:　　　　　　$a \leftarrow \Re\{T_I(k, n) \times g(n, n)\}$
9:　　　　　　**if** $a \leq 0$ **then**
10:　　　　　　　$NegSum \leftarrow NegSum - a$
11:　　　　　　**else**
12:　　　　　　　$PosSum \leftarrow PosSum + a$
13:　　　　　　**end if**
14:　　　　**end for**
15:　　　　**if** $NegSum \geq PosSum$ **then**
16:　　　　　　$LargerSum \leftarrow NegSum$
17:　　　　**else**
18:　　　　　　$LargerSum \leftarrow PosSum$
19:　　　　**end if**
20:　　　　$g(n, n) \leftarrow g(n, n) \div LargerSum$
21:　　**end for**
22:　　$[T_I] \leftarrow [T_I] \times [g]$
23:　　$[T_V] \leftarrow [T_I]^{-1^T}$
24:　　**return** ($[T_V]$, $[T_I]$)
25: **end procedure**

---

found to be:

$$[Z_{cM}] = diag \begin{bmatrix} 50.057 - j0.0667 \\ 101.3070 - j0.0309 \end{bmatrix} \Omega \qquad (51a)$$

$$[Z_{cM}] = diag \begin{bmatrix} 770.9380 - j0.0204 \\ 65.1615 + j0.0259 \\ 49.8871 + 0.0365 \\ 26.8548 + j0.0160 \end{bmatrix} \Omega \qquad (51b)$$

where *diag* indicates the entries on the lead diagonal of a diagonal matrix, in which the off-diagonal entries are zero. These data are compared with those obtained using other methods in Table 1, where it may be observed that in general these values are significantly different from those produced by HFSS as compared with the method proposed in this work.

APPENDIX C LAYOUT OF ODD-MODE FEED TRANSITION

Since the VNA interfaces with its test devices via coaxial modes, an inherent unbalance of currents will always develop whenever a transition to planar TLs is used. In order to excite a pure balanced mode for the odd-mode feedline of Sec. V, two connections are used to excite a single mode in a differential fashion [24]. While electrically small, this transition section still needs to be precisely designed in order to achieve the low levels of reflection required for this work. This design consists of two individual 61 Ω slotlines (SLs) which merge into one 100 Ω line. 61 Ω was chosen as the SL impedance instead of the ideal 50 Ω, due to the fact that, on the chosen substrate, the required SL gap would be smaller
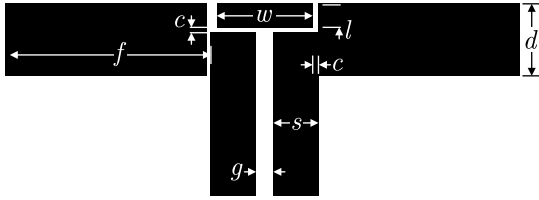
FIGURE 11. Geometric parameters of the CPS feed to SMA connectors transition.
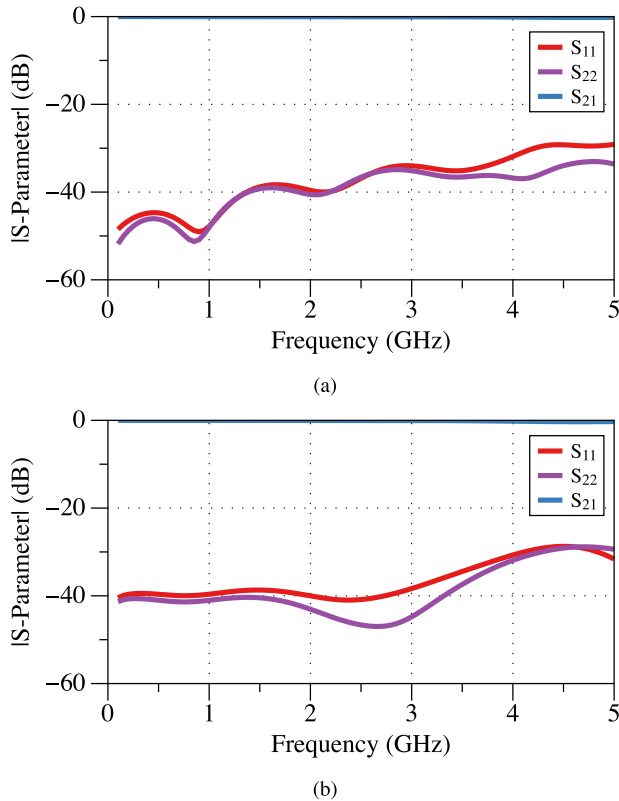

FIGURE 12. Simulated scattering parameters of the SMA connectors and transition regions for: (a) even-mode excitation, (b) odd-mode excitation.

than 50 μm, which was deemed the smallest that could be reliably fabricated via the LPKF ProtoLaser U3 laser milling machine. Even still, a return loss of greater than 29 dB was achieved for the transition. The geometric parameters of the feed section are given in Fig. 11, where $c = 0.05$ mm, $w = 5.00$ mm, $f = 4.00$ mm, $l = 1.05$ mm, $d = 2.50$ mm, $g = 0.20$ mm, $s = 1.40$ mm. The simulated magnitudes of the scattering parameters of these feed-line transitions are shown in Fig. 12, where the SMA connectors are at port 2 and the waveport-excited TLs at port 1. It may be observed that excellent matching is achieved; the scattering parameters of the even-mode MS transition (SMA to MS) is also shown for comparison purposes, showing comparable matching levels.

APPENDIX D TERMINAL-TO-MODAL CONVERSION OF SCATTERING PARAMETERS
When the terminal-domain impedances of all ports are the same, simple voltage-based scattering parameters may be
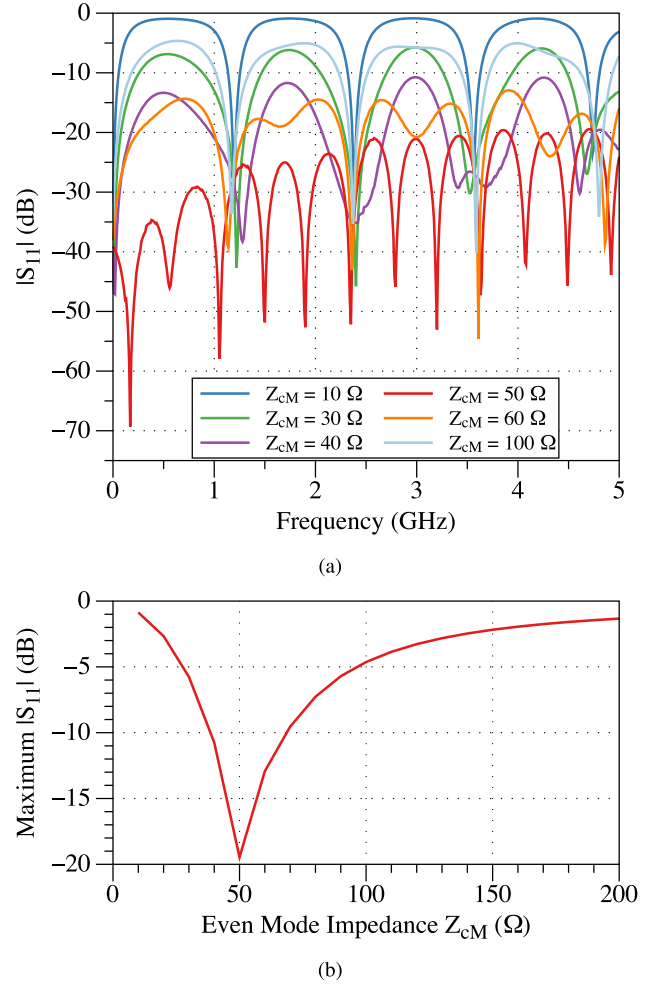

FIGURE 13. S_{11} of equivalent even-mode circuit models with various MTL modal impedances (Z_{cM}): (a) frequency-domain data, (b) maximum S_{11} over the frequency range as a function of modal impedance.

used (as opposed to the more general power-wave scattering parameters needed for the case of differing impedances). This formulation may be expressed as:

$$\vec{V}_{NT}^{-} = [S_T] \, \vec{V}_{NT}^{+} \tag{52}$$

where $\vec{V}_{NT}$ are the vectors of voltages at all ports of a multi-port network, and $[S_T]$ are the terminal-domain scattering parameters. Noting that the modal-terminal transformations apply to single travelling waves as well (i.e., $\vec{V}_T^{+}$ or $\vec{V}_T^{-}$, instead of just their sum $\vec{V}_T$), yields the relation:

$$\vec{V}_T^{+} = [T_V] \, \vec{V}_M^{+} \tag{53a}$$
$$\vec{V}_T^{-} = [T_V] \, \vec{V}_M^{-} \tag{53b}$$

where for a given MTL,

$$\vec{V}_{NT}^{+} = \left[\vec{V}_T^{+}, \vec{V}_T^{+} \right] \tag{54a}$$
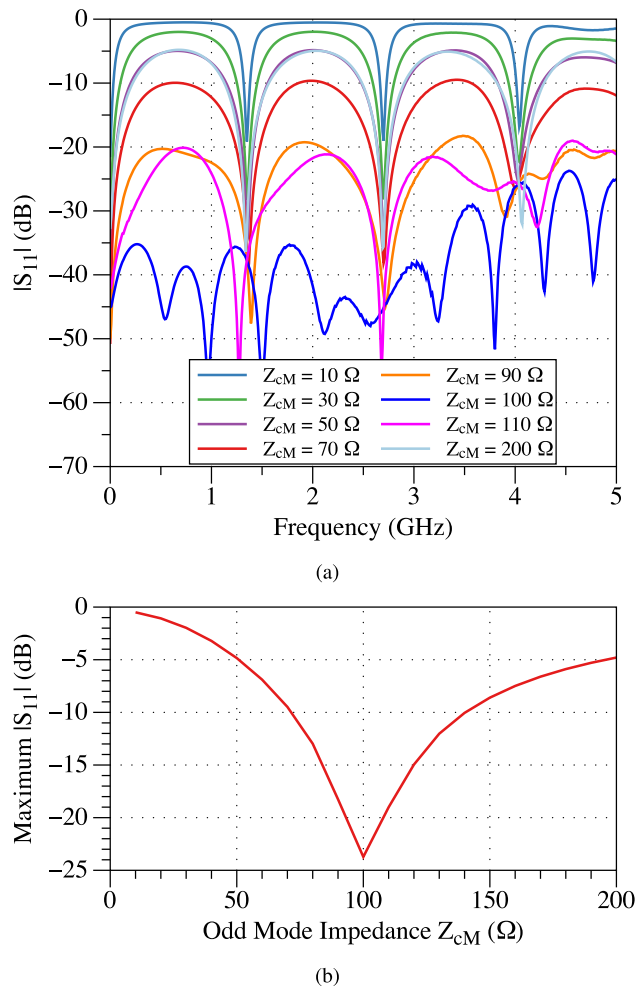$$\vec{V}_{NT}^{-} = \left[\vec{V}_T^{-}, \vec{V}_T^{-} \right] \tag{54b}$$

(a)

(b)

FIGURE 14. S_{11} of equivalent odd-mode circuit models with various MTL modal impedances (Z_{cM}): (a) frequency-domain data, (b) maximum S_{11} over the frequency range as a function of modal impedance.

If each of (53) details the terminal-modal transformations at a each end of the TL, then this network may be transformed by substituting (53) back into (52):

$$\begin{bmatrix} [T_V] & 0 \\ 0 & [T_V] \end{bmatrix} \vec{V}_M^- = [S_T] \begin{bmatrix} [T_V] & 0 \\ 0 & [T_V] \end{bmatrix} \vec{V}_M^+ \quad (55)$$

such that we may define

$$[S_M] = \begin{bmatrix} [T_V] & 0 \\ 0 & [T_V] \end{bmatrix}^{-1} [S_T] \begin{bmatrix} [T_V] & 0 \\ 0 & [T_V] \end{bmatrix} \quad (56)$$

This is a common transformation found in the literature, especially those concerning the measurement of balanced/single-ended scattering parameters.

It should be noted that the transformation matrix $[T_V]$ does not need to be scaled in this case, since any scale factors applied to the mode definitions will cancel out; however, for a more general analysis involving power waves, this will not be the case – and scaling is required.

APPENDIX E PARAMETRIC SWEEPS OF MODAL IMPEDANCE AND ASSOCIATED SCATTERING DATA

In order to alleviate concerns that the chosen two impedances may have coincidentally matched or mismatched, this appendix provides additional scattering data, demonstrating that the predicted modal impedances are indeed the best match for the designed two-conductor feed lines, and that MTLs with other impedances scatter as expected. Figs. 3b and 4b detail the layout of the modal-domain circuits for the even- and odd-mode feeds, respectively.

The scattering parameters of these circuits are presented for various values of the characteristic impedances (Z_{cM}) of the MTL sections (blue, labelled "Even Mode" and "Odd Mode") in Figs. 13a and 14a, respectively. Additionally, the maximum $|S_{11}|$ data over the entire frequency range are plotted in Figs. 13b and 14b.

The Z_{cM} values corresponding to the minimum $|S_{11}|$ indicate the presence of a matched impedance – since these optimal impedance values are indeed only those predicted by the proposed method (50 Ω and 100 Ω for the even and odd modes, respectively), coincidence is effectively ruled out as a factor in producing a matched system.

REFERENCES

[1] C. R. Paul, *Analysis of Multiconductor Transmission Lines*, 2nd ed. Hoboken, NJ, USA: Wiley, 2008.

[2] J. A. B. Faria, *Multiconductor Transmission-Line Structures: Modal Analysis Techniques*. Hoboken, NJ, USA: Wiley, 1993.

[3] K. D. Marx, "Propagation modes, equivalent circuits, and characteristic terminations for multiconductor transmission lines with inhomogeneous dielectrics," *IEEE Trans. Microw. Theory Techn.*, vol. 21, no. 7, pp. 450–457, Jul. 1973.

[4] L. Carin and K. J. Webb, "Characteristic impedance of multilevel, multiconductor hybrid mode microstrip," *IEEE Trans. Magn.*, vol. 25, no. 4, pp. 2947–2949, Jul. 1989.

[5] D. F. Williams, "Multiconductor transmission line characterization," *IEEE Trans. Compon., Packag., Manuf. Technol.*, vol. 20, no. 2, pp. 129–132, May 1997.

[6] M. S. Alam, M. Koshiba, K. Hirayama, and Y. Hayashi, "Hybrid-mode analysis of multilayered and multiconductor transmission lines," *IEEE Trans. Microw. Theory Techn.*, vol. 45, no. 2, pp. 205–211, 1997.

[7] C. R. Paul, "Decoupling the multiconductor transmission line equations," *IEEE Trans. Microw. Theory Techn.*, vol. 44, no. 8, pp. 1429–1440, 1996.

[8] J. A. B. Faria, "A new generalized modal analysis theory for nonuniform multiconductor transmission lines," *IEEE Trans. Power Syst.*, vol. 19, no. 2, pp. 926–933, May 2004.

[9] G. G. Gentili and M. Salazar-Palma, "The definition and computation of modal characteristic impedance in quasi-TEM coupled transmission lines," *IEEE Trans. Microw. Theory Techn.*, vol. 43, no. 2, pp. 338–343, 1995.

[10] G.-T. Lei, G.-W. Pan, and B. K. Gilbert, "Examination, clarification, and simplification of modal decoupling method for multiconductor transmission lines," *IEEE Trans. Microw. Theory Techn.*, vol. 43, no. 9, pp. 2090–2100, 1995.

[11] J. A. B. Faria, "Nonuniqueness of modal transformations for multiconductor transmission line problems," *Int. Trans. Electr. Energy Syst.*, vol. 27, no. 8, p. e2342, Aug. 2017.

[12] J. He and Z. F. Fu, *Modal Analysis*, 1st ed. Woburn, MA, USA: Butterworth-Heinemann, 2001.

[13] F. Elek and G. V. Eleftheriades, "Dispersion analysis of the shielded sievenpiper structure using multiconductor transmission-line theory," *IEEE Microw. Wireless Compon. Lett.*, vol. 14, no. 9, pp. 434–436, Sep. 2004.

[14] F. Bongard, J. Perruisseau-Carrier, and J. R. Mosig, "Enhanced periodic structure analysis based on a multiconductor transmission line model and application to metamaterials," *IEEE Trans. Microw. Theory Techn.*, vol. 57, no. 11, pp. 2715–2726, Nov. 2009.

[15] R. Islam and G. V. Eleftheriades, "On the independence of the excitation of complex modes in isotropic structures," *IEEE Trans. Antennas Propag.*, vol. 58, no. 5, pp. 1567–1578, May 2010.

[16] K. Payandehjoo, A. Tavallaee, and R. Abhari, "Analysis of shielded electromagnetic bandgap structures using multiconductor transmission-line theory," *IEEE Trans. Adv. Packag.*, vol. 33, no. 1, pp. 236–245, Feb. 2010.

[17] S. Barth and A. K. Iyer, "A miniaturized uniplanar metamaterial-based EBG for parallel-plate mode suppression," *IEEE Trans. Microw. Theory Techn.*, vol. 64, no. 4, pp. 1176–1185, Apr. 2016.

[18] A. M. Nicolson and G. F. Ross, "Measurement of the intrinsic properties of materials by time-domain techniques," *IEEE Trans. Instrum. Meas.*, vol. 19, no. 4, pp. 377–382, Nov. 1970.

[19] W. B. Weir, "Automatic measurement of complex dielectric constant and permeability at microwave frequencies," *Proc. IEEE*, vol. 62, no. 1, pp. 33–36, 1974.

[20] J. O. Scanlan, "Theory of microwave coupled-line networks," *Proc. IEEE*, vol. 68, no. 2, pp. 209–231, 1980.

[21] B. J. A. Faria and B. J. F. da Silva, "Irregular eigenvalues in the analysis of multimodal propagation," in *Proc. 8th Power Syst. Comput. Conf.*, Helsinki, Finland, Aug. 1984, pp. 760–764.

[22] D. F. Williams, L. A. Hayden, and R. B. Marks, "A complete multimode equivalent-circuit theory for electrical design," *J. Res. Nat. Inst. Standards Technol.*, vol. 102, no. 4, pp. 405–423, 1997.

[23] J. A. B. Faria and J. F. B. da Silva, "Wave propagation in polyphase transmission lines a general solution to include cases where ordinary modal theory fails," *IEEE Trans. Power Del.*, vol. 1, no. 2, pp. 182–189, 1986.

[24] D. F. Williams, J. E. Rogers, and C. L. Holloway, "Multiconductor transmission-line characterization: Representations, approximations, and accuracy," *IEEE Trans. Microw. Theory Techn.*, vol. 47, no. 4, pp. 403–409, Apr. 1999.

[25] G. W. Slade and K. J. Webb, "Computation of characteristic impedance for multiple microstrip transmission lines using a vector finite element method," *IEEE Trans. Microw. Theory Techn.*, vol. 40, no. 1, pp. 34–40, 1992.

[26] V. K. Tripathi and H. Lee, "Spectral-domain computation of characteristic impedances and multiport parameters of multiple coupled microstrip lines," *IEEE Trans. Microw. Theory Techn.*, vol. 37, no. 1, pp. 215–221, 1989.

[27] R. A. Horn and C. R. Johnson, *Matrix Analysis*, 2nd ed. Cambridge, U.K.: Cambridge Univ. Press, 2013.

[28] F.-Y. Chang, "Transient analysis of lossless coupled transmission lines in a nonhomogeneous dielectric medium," *IEEE Trans. Microw. Theory Techn.*, vol. 18, no. 9, pp. 616–626, 1970.

[29] F. Grassi, Y. Yang, X. Wu, G. Spadacini, and S. A. Pignari, "On mode conversion in geometrically unbalanced differential lines and its analogy with crosstalk," *IEEE Trans. Electromagn. Compat.*, vol. 57, no. 2, pp. 283–291, Apr. 2015.

[30] G. Ghione, I. Maio, and G. Vecchi, "Modeling of multiconductor buses and analysis of crosstalk, propagation delay and pulse distortion in high speed GaAs logic circuits," *IEEE Trans. Microw. Theory Techn.*, vol. 37, no. 3, pp. 445–456, Mar. 1989.

STUART BARTH (Member, IEEE) received the B.Sc. and M.Sc. degrees in electrical engineering from the University of Alberta, Edmonton, AB, Canada, in 2012 and 2015, respectively, where he is currently pursuing the Ph.D. degree.

His current research interests include the study of fundamental electromagnetic theory, multiconductor transmission line-based metamaterials and microwave circuits, dispersion engineering, and antenna radiation-pattern shaping.

Mr. Barth received the IEEE AP-S Pre-Doctoral Research Award in 2014 and the IEEE AP-S Doctoral Research Grant in 2016 for his ongoing research into electromagnetic bandgap structures for antenna and waveguide applications. He serves as an Officer for the IEEE Northern Canada Section and its MTT-S/AP-S Joint Chapter.

ASHWIN K. IYER (Senior Member, IEEE) received the B.A.Sc. (Hons.), M.A.Sc., and Ph.D. degrees in electrical engineering from the University of Toronto, Toronto, ON, Canada, in 2001, 2003, and 2009, respectively, where he was involved in the discovery and development of the negative-refractive-index transmission-line approach to metamaterial design and the realization of metamaterial lenses for free-space microwave subdiffraction imaging. He is currently an Associate Professor with the Department of Electrical and Computer Engineering, University of Alberta, Edmonton, AB, Canada, where he leads a team of graduate students investigating novel RF/microwave circuits and techniques, fundamental electromagnetic theory, antennas, and engineered metamaterials, with an emphasis on their applications to microwave and optical devices, defense technologies, and biomedicine. He has coauthored a number of highly cited articles and four book chapters on the subject of metamaterials. He is a member of the IEEE AP-S Education Committee. He was a recipient of the IEEE AP-S R. W. P. King Award in 2008, the IEEE AP-S Donald G. Dudley Jr. Undergraduate Teaching Award in 2015, the University of Alberta Provost's Award for Early Achievement of Excellence in Undergraduate Teaching in 2014, and the University of Alberta Rutherford Award for Excellence in Undergraduate Teaching in 2018. His students are the recipients of several major national and international awards for their research. He serves as the Chair for the IEEE Northern Canada Section's Award-Winning Joint Chapter of the AP-S and MTT-S. He served as a Technical Program Committee Co-Chair for the 2020 AP-S/URSI International Symposium. From 2012 to 2018, he was an Associate Editor of the IEEE TRANSACTIONS ON ANTENNAS AND PROPAGATION. He also serves as a Track Editor. He was also the Guest Editor of the IEEE TRANSACTIONS ON ANTENNAS AND PROPAGATION Special Issue on Recent Advances in Metamaterials and Metasurfaces. He is a Registered Member of the Association of Professional Engineers and Geoscientists of Alberta.

• • •